

Vertical-Cavity Surface-Emitting Lasers for Ultra-High Speed Photonics

Moustafa Ahmed^{1*}, Hameeda R. Ibrahim^{1,2} and Fumio Koyama²

¹Department of Physics, Faculty of Science, Minia University, 61519 Minia, Egypt.

²Precision & Intelligence Laboratory, Tokyo Institute of Technology, Japan.

Abstract

We propose a vertical-cavity surface-emitting laser (VCSEL) with a transverse-coupled-cavity (TCC) for larger enhancement of the modulation bandwidth for use in ultra-high speed photonics. The dynamics of the TCC-VCSEL are analyzed over three characteristic regimes of OFB that correspond to continuous wave (CW) operation, pulsation and chaos, depending on the coupling ratio between the VCSEL and feedback cavities. The intensity noise is evaluated in terms of the frequency spectrum of the relative intensity noise (RIN) and the carrier to noise ratio (CNR). The results show strong lateral OFB can boost the modulation bandwidth to frequencies approaching 70 GHz. The free-running TCC-VCSEL follows CW operation, pulsation and then chaos with the increase of coupling ratio. Under weak OFB, RIN is lowest under CW operation, increases under the pulsing, and is pronounced in the chaos region. A TCC VCSEL with a short feedback cavity shows stable CW operation without a noticeable change in either RIN or CNR.

1. Introduction

VCSELs have small size, low cost, high-speed operation, low power consumption, and also can be fabricated into arrays [1,2]. These advantages make VCSELs attracting much attention for use in photonics, e.g. fiber communications, radio-over fiber networks, optical data centers. Because the modern versions of these applications require dense traffic and high-speed transmission, the development of high speed VCSELs is a key issue. Various approaches have been reported to increase the speed of VCSELs. Subjecting the semiconductor laser to external OFB is an efficient technique to enhance the modulation bandwidth. OFB has been used for increasing the bandwidth frequency of VCSELs [3, 4], linewidth narrowing [5, 6], decreasing of frequency chirp [7], and stability of mode operation [8]. 60% improvement of the modulation bandwidth is expected by Dalir and Koyama using TCC feedback [9,10]. Ahmed et al. [11] analyzed the modulation characteristics of TCC VCSELs and explained the bandwidth improvement as a type of photon-photon resonance.

Lang and Kobgyashi [12] incorporated the OFB effect in the rate equation model of semiconductor laser by adding a time delayed feedback term. But this model is used only for weak and intermediate value of OFB; it was commonly followed by theoretical groups. Abdulrhmann et al. [13] improved the time-delay model of Lang-Kobgyashi to analyze and classify laser operation, dynamics under strong OFB. On the other hand, the operation stability and noise of the laser is an important issue for applications. Despite of the advantages of applying OFB to VCSEL, OFB may change CW operation dynamic to dynamics in the form of periodic oscillation, period doubling, quasi-periodicity and even chaos [14], depending on the intensity and phase of the OFB radiation. These instabilities deteriorate the noise performance of the device [15]. Analysis of noise in VCSELs under OFB is then necessary for developing high-speed VCSELs with high performance for application in high-speed photonics.

In this work, we present the modeling of TCC VCSELs, demonstrating how strong lateral optical feedback can enhance the modulation bandwidth to record 70 GHz. OFB is treated as time delay of the electric field of the slow light in the TCC with multiple round trips. Also, we present computer simulation of the intensity noise in these VCSELs, and report on a design for low noise operation. The intensity noise is determined according to RIN and CNR.

2. Theoretical model

The proposed TCC-VCSEL is sketched in Fig. 1. The VCSEL is integrated with an external cavity out of a bow-tie oxide aperture [9]. In the lateral direction, light slowed down and move in zigzag inside the VCSEL cavity with angle $\Phi \sim 90^\circ$ in the TCC. In the TCC of length L_C , the slow light is totally reflected back inside VCSEL cavity. The lateral light travels in the TCC with a round trip time of $\tau = 2n_g L_C / c$, where $n_g = fn$ is the group velocity, n is the average material refractive index, and f is the slowdown factor of light inside TCC. After each round trip, the laser light is injected into the VCSEL cavity with a coupling ratio η . OFB is treated as time delay of the electric field of the slow light in the TTC with multiple round trips. The present model of lateral OFB in the TCC VCSEL is treated by using a time-delay rate equation model of edge-emitting lasers under strong OFB in [13].

The time-delay rate equation model is presented according to following rate equations of the carrier number $N(t)$ injected inside the active region, emitted photon number $S(t)$, and the optical phase $\theta(t)$,

$$\frac{dN}{dt} = \frac{\eta_i}{e} I(t) - \frac{N}{\tau_s} - GS + f_N(t) \quad (1)$$

$$\frac{dS}{dt} = \left[\Gamma G - \frac{1}{\tau_p} + \frac{v_g}{W} \ln|U| \right] S + \Gamma R_{sp} + f_S(t) \quad (2)$$

$$\frac{d\theta}{dt} = \frac{1}{2} \left(\alpha \Gamma \frac{a}{V} (N - N_{th}) - \frac{c}{n_g W} \varphi \right) + f_\theta(t) \quad (3)$$

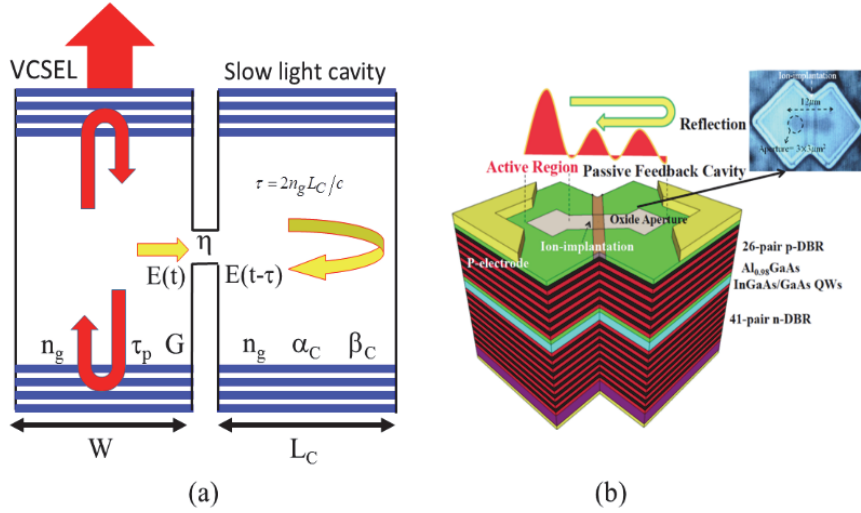


Fig. 1. Scheme of VCSEL with TCC: (a) theoretical model and (b) structure.

In the above equations, Γ is the confinement factor, V volume of the active region, G optical gain, a differential gain, R_{sp} rate of spontaneous emission. N_T transparency electron number, η_i the injection efficiency, ε gain suppression coefficient, τ_p photon lifetime, τ_s electron lifetime due to spontaneous emission, and N_{th} electron number at threshold. The lateral OFB is included in the time-delay function $U(t-\tau)$ as

$$U = 1 + \frac{\eta}{1-\eta} \sum_k \sqrt{1-\eta}^k e^{-2k\alpha_C L_C} e^{-j2k\beta_C L_C} \sqrt{\frac{S(t-k\tau)}{S(t)}} e^{j\theta(t-k\tau) - j\theta(t)} \quad (4)$$

where $\theta(t) - \theta(t-k\tau)$ is the deflection in the optical phase in round trip k due to frequency chirp, while the terms $\exp(-2k\alpha_C L_C)$ and $\exp(-j2k\beta_C L_C)$ represent the loss and phase delay suffered by the slow light in round trip m , respectively. $\alpha_C = f\alpha_m$ and $\beta_C = 2\pi n/(\lambda f)$ are the optical loss and propagation constant, respectively.

The direct current modulation of the device is described as

$$I(t) = I_b + I_m \sin(2\pi f_m t) , \quad (5)$$

where I_b is the DC current and I_m is the modulation current. The modulation depth is defined as $m = I_m / I_b$. Finally $F_N(t)$, $F_S(t)$ and $F_\theta(t)$ in Eqs. (1) – (3), respectively, and are given by [16]

$$f_s(t) = \sqrt{\frac{2 R_{sp} \Gamma S(t)}{\Delta t}} \cdot x_s \quad (6)$$

$$f_N(t) = \sqrt{\frac{2 N(t)}{\tau_s \Delta t}} \cdot x_n - \sqrt{\frac{2 R_{sp} S(t)}{\Delta t}} \cdot x_s \quad (7)$$

$$f_\theta = \sqrt{\frac{R_{sp} \Gamma}{2 S(t) \Delta t}} \cdot x_\theta \quad (7)$$

where x_s , x_n and x_θ are three independent random numbers with Gaussian probability distributions.

The frequency content of intensity fluctuations is measured in terms of RIN, which is calculated as the Fourier transformation of the photon number fluctuations $\delta S(t) = S(t) - S_b$ around the bias value S_b . Over a finite time T , RIN is given as [16]

$$RIN = \frac{1}{S_b^2} \left\{ \frac{1}{T} \left| \int_0^T \delta S(t) e^{-j2\pi f t} dt \right|^2 \right\} \quad (8)$$

For LF-RIN, we take the average values of the RIN components over frequencies lower than than 100 kHz.

1. Procedures of Numerical Calculations

To explain the modulation bandwidth enhancement and dynamics of TCC-VCSEL, we use the fourth-order Runge-Kutta method to solve the rate equations numerically. Also we plot the bifurcation diagram to study the effect of the amount of OFB on VCSEL dynamics. The time step is taken as 2ps for high accuracy. We use multiple round trips in our calculations with $k_{max} = 6$ rounds. First, we solve the integration without OFB, i.e., with time between 0 and τ . The values of $S(t=0 \rightarrow \tau)$ and $\theta(t=0 \rightarrow \tau)$ are then stored for use as values of time delayed $S(t \rightarrow \tau)$ and $\theta(t \rightarrow \tau)$ for integration of the rate equations over the period $t=(t \rightarrow 2\tau)$ with OFB terms and so on for all round trips. The total calculation time should be higher than

1.1 μs to reach the stable operation of laser [14]. The numerical values of the laser parameters used in the calculations are listed in table 1.

Table 1. VCSEL parameters and their numerical values [17].

Parameter	Value
Active region refractive index of n	3.3
Material loss of active region α_m	10 cm^{-1}
Slow down factor f	50
Volume of active region V	$1.76 \times 10^{-19} \text{ m}^3$
Width of active region W	$4 \mu\text{m}$
Differential gain a	$3.64 \times 10^{-12} \text{ m}^3 \text{ s}^{-1}$
Confinement factor Γ	0.0382
Electron number at transparency N_T	3.17×10^5
Gain suppression coefficient ε	$1.5 \times 10^{-5} \text{ s}^{-1}$
Lifetime of photon τ_p	2 ps
Spontaneous emission factor R_{sp}'	$1.16 \times 10^{10} \text{ s}^{-1}$
Efficiency of injection η_i	0.8
Electron lifetime τ_s	1.5 ns
Linewidth enhancement factor α	2

2. Results and discussion

2.1. Improving modulation bandwidth

We present in Fig. 2 the results on the bandwidth enhancement of VCSEL induced by coupling it with the TCC. The figure plots the IM response when the modulation index is $m = 0.01$ under different values of the coupling ratio η when $L_C = 20 \mu\text{m}$. The figure shows that the IM response of the VCSEL without feedback has a peak at the carrier-photon resonance (CPR) frequency of 12 GHz, and bandwidth frequency of $f_{3dB0} = 24 \text{ GHz}$. The plotted examples of the IM responses have improved modulation characteristics over that of the

conventional VCSEL. The modulation bandwidth improves to $f_{3dB} = 33.5$ GHz when $\eta = 0.5$, due to shifts of CPR frequency to the higher frequency of $f_m = 16$ GHz, and the peak of CPR reaches ~ 5 dB. When the coupling ratio increase to $\eta = 0.7$, f_{3dB} increases further to 42 GHz; that is, f_{3dB} 79 higher than that of the covenantal VCSEL. This result is much larger than the percentage of 60% reported in [10]. The IM response does not drops below the -3 dB level; but we can see another peak of value ~ 1.4 dB at the mm-wave frequency of $f_m = 39$ GHz. Under very strong OFB of $\eta = 0.96$, the figure indicates further improvement of the IM-response; the mm-wave peak shifts to frequency of 49.6 GHz, which is much higher than that of the CPR peak. This IM response can be considered as a type of extended CPR to the mm-wave region [11].

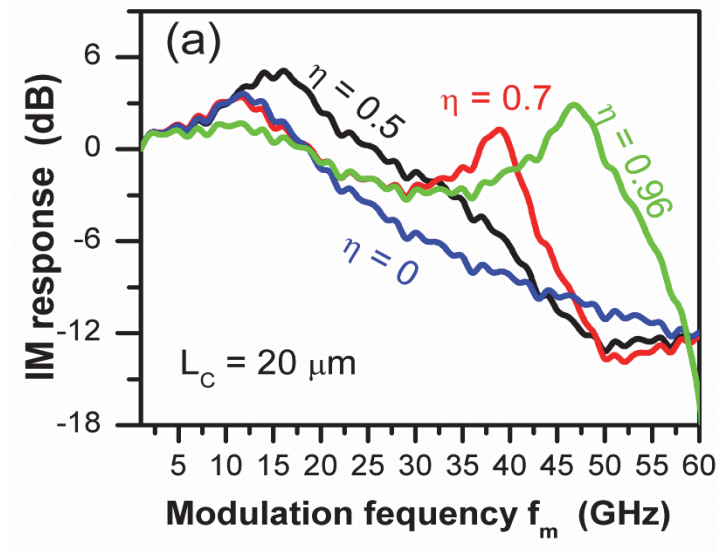


Fig. 2. Frequency spectrum of the IM responses under different values of η : with CPR.

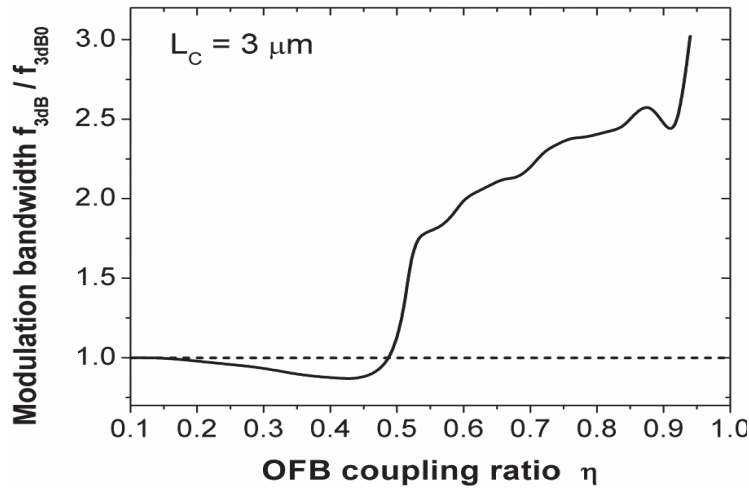


Fig. 3. The modulation bandwidth frequency f_{3dB} as a function of the coupling ratio η when the TCC length is $L_C = 3 \mu\text{m}$.

Figure 3 plots the relation between the coupling coefficient η and the modulation bandwidth f_{3dB} when the length of TCC is $L_C = 3 \mu\text{m}$. When the coupling ratio is $\eta = 0.45$, the figure indicates that f_{3dB} is dropped to $0.87 f_{3dB0}$ with the increase in the OFB strength. When the coupling ratio increases further, the figure shows large enhancement in f_{3dB} , indicating that the strong OFB has a large effect to induce high-modulation bandwidth frequencies. When $\eta = 0.94$ the modulation bandwidth f_{3dB} is enhanced more up to $3f_{3dB0}$.

2.2. Dynamics and analysis of noise in TCC-VCSEL

Before presenting the results on the noise subject, we explain the characteristics of the TCC VCSEL dynamics under OFB, and show the induced dynamics classes. For this purpose, we use the bifurcation diagram of the laser intensity. The bifurcation diagram is constructed at a fixed injection current by sampling the peaks S_{peak} of the time-varying photon number, and plotting these peaks (normalized by the bias value S_b) as a function of the coupling ratio η . Figure 4 plots this bifurcation diagrams when the length of TCC is $L_C = 15 \mu\text{m}$. The figure indicates that the operation of the TCC-VCSEL is stable CW when the OFB is as weak as $\eta < 0.35$. The dynamics of the CW operation are presented in the figure as single circuits at $S_{peak}/S_b=1$. Then the VCSEL emits periodic oscillations starting from $\eta=0.34$. Many closely spaced points at each η in the figure represent this pulsation. For intimate values of η , more than two oscillation periods are induced, attracting the VCSEL to the chaotic region. With the increase in η , the VCSEL thereafter catches again to stable CW operation when $\eta > 0.63$.

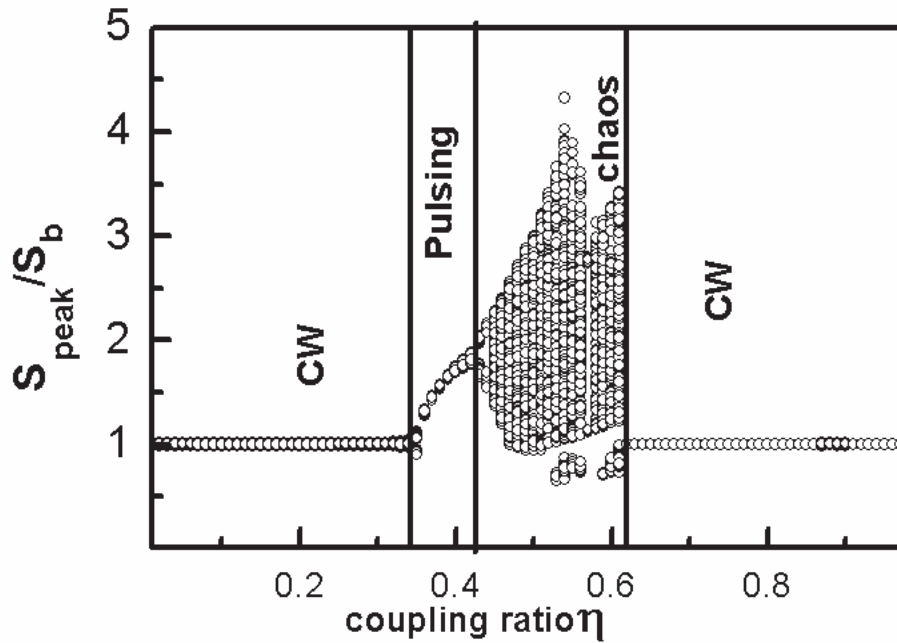


Fig. 4 Bifurcation diagram of $S(t)$ with η when $L_C = 15\mu\text{m}$.

2.3. Characteristics of TCC-VCSELs dynamic states

Typical signal shapes of the TCC-VCSEL dynamic types and frequency spectra of RIN (dB/Hz) are shown in figures 5(a) – (d) and 6(a) – (d), respectively. These figures correspond to $\eta = 0.2$ (weak OFB), $\eta = 0.4$ (intermediate OFB), $\eta = 0.54$ (rather intermediate OFB), and $\eta = 0.9$ (strong OFB). Figure 5(a) characterizes the weak regime of OFB with CW operation, and shows that the emitted photon number $S(t)$ is almost coincident with that of the conventional VCSEL. Figure 5(b) corresponds to rather intermediate value of the coupling ratio $\eta = 0.4$, and characterizes the periodic oscillation; $S(t)$ oscillates with a period close to $1/f_r$ where f_r is CPR frequency of the VCSEL. In this dynamic type, OFB is strong enough to make the relaxation oscillation undamped, and pulses are then generated. Figure 5(c) plots the extreme unstable dynamic state of chaos in the intermediate range of OFB ($\eta = 0.54$). This state is characterized by an irregular variation of $S(t)$ with the time variation. These characteristics agree with those obtained by Ahmed et al. in [11, 18]. Under very strong OFB with $\eta = 0.9$, Fig. 5(d) shows that the CW operation is re-generated. The characteristics of this CW operation are almost coincident with those of the conventional VCSEL. These characteristics agrees with the expectations by Ahmed et al. [18]

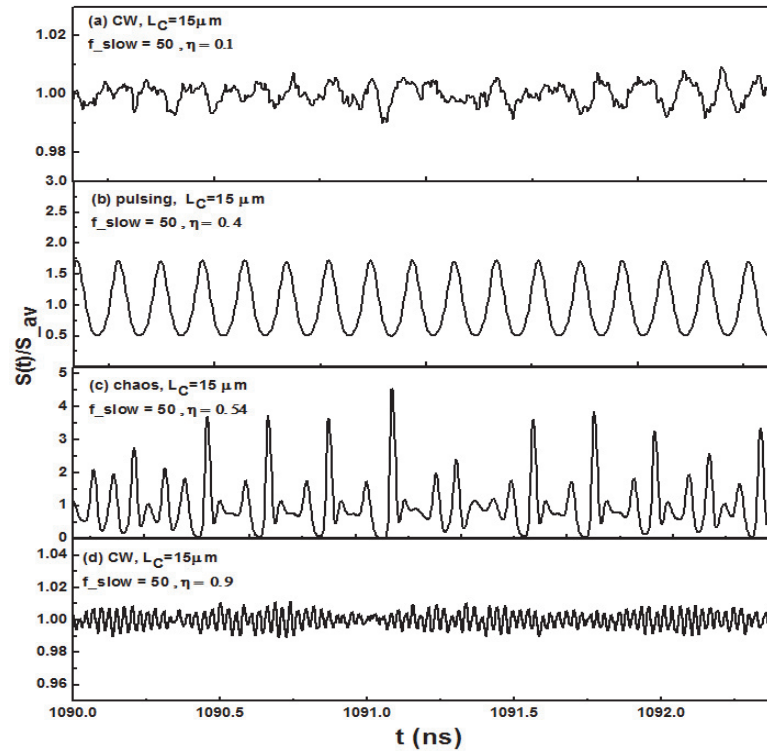


Fig. 5. Signal characteristics of (a) CW ($\eta = 0.2$), (b) pulsing ($\eta = 0.4$), (c) chaos ($\eta = 0.54$), and (d) CW ($\eta = 0.9$) when $L_C = 15\mu\text{m}$.

Figures 6(a) – (d) show the frequency spectra of RIN that correspond to the signal shapes in Fig. 5(a) – (d), respectively. The RIN spectrum of the VCSEL without OFB is also presented in the figures plotted by dashed line for comparison. Figure 6(a) corresponds to the CW operation, which characterizes the weak regime of coupling ratio $\eta = 0.1$. The RIN spectrum presented in this figure is comparable to that of the conventional VCSEL, exhibiting the pronounced peak around the CPR frequency. It implies that the weak value of coupling ratio is not sufficient to change the relaxation oscillation frequency of TCC-VCSEL. Figure 6(b) corresponds to the intermediate value of the coupling ratio $\eta = 0.4$, which is characterized by period-1 oscillations. The RIN spectrum has a very sharp peak around a frequency comparable to the CPR frequency and other peaks at the higher harmonics. These characteristics agree with those reported by Ahmed et al. [19]. Figure 6(c) plots the RIN spectrum of the chaotic dynamics induced by OFB when $\eta = 0.54$. The figure shows the noisiest chaotic state suffered by the VCSEL in the intermediate range of OFB. In this case, RIN is 40 dB higher than that of the VCSEL without OFB. Figure 6(d) shows the RIN spectrum characterizing the stable CW operation in the regime of strong OFB ($\eta = 0.9$). This RIN spectrum is almost the same as that of the CW operation of $\eta = 0.1$.

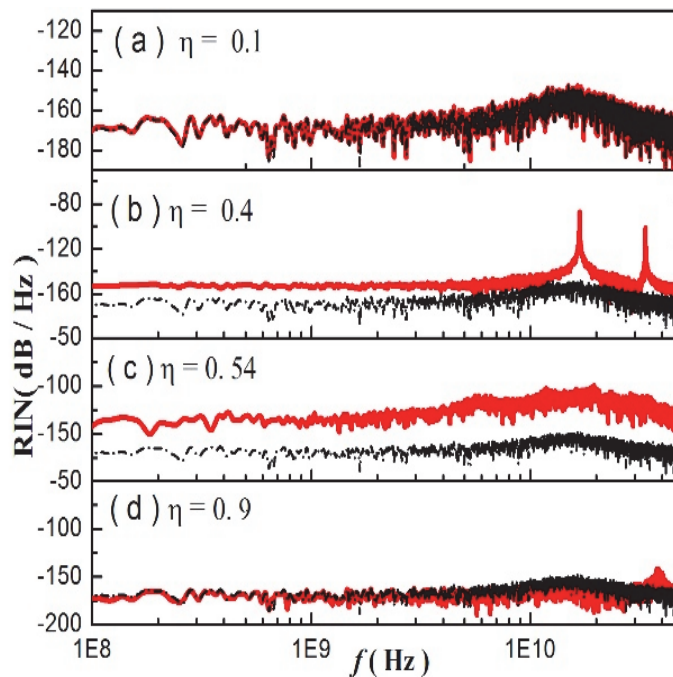


Fig. 6. RIN spectrum of (a) CW ($\eta = 0.1$), (b) pulsing ($\eta = 0.4$), (c) chaos ($\eta = 0.54$) and (d) CW ($\eta = 0.9$) when $L_C = 15\mu\text{m}$. The RIN spectrum of the solitary VCSEL is plotted by the dashed line.

We investigate the variation of noise with the strength of OFB. The noise is calculated in terms the low-frequency RIN (LF-RIN) as well as CNR. The results are plotted in Fig. 7, which plots CNR on the left-hand axis and LF-RIN on the right-hand axis as functions of coupling ratio η . The figure indicates that LF-RIN is lowest under CW operation, and increases slowly under the period-1 oscillations. When η increases beyond 0.41, LF-RIN increases and is pronounced in the chaos region. When $\eta > 0.63$, LF-RIN drops to lower levels again under the CW operations. The figure shows also that under CW operation, CNR is almost in the same level as that of the VCSEL without OFB. CNR decreases with the increase in the coupling ratio η under the period-1 oscillation and reaches to the lowest values under the chaotic dynamics before restoring the upper limit of the strong OFB-induced CW operation.

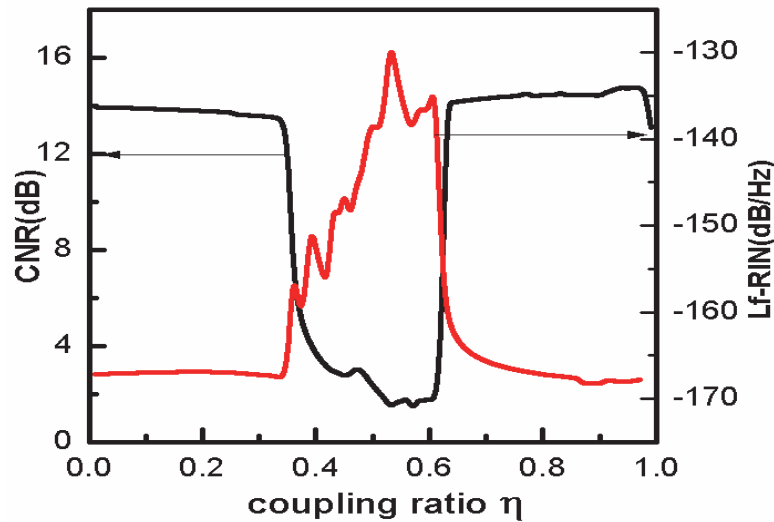


Fig. 7. Variation of LF-RN and CNR with η when $L_C = 15\mu\text{m}$.

2.4. Influence of TCC length on noise performance of TCC VCSEL

In this subsection, we give attention to find out the optimum length of the TCC that corresponds to best noise performance of the TCC VCSEL. In figures 8(a) and (b), we plot both CNR and LF-RIN as functions of the length T_C of TCC cavity, respectively, under different strengths of OFB of $\eta = 0.1, 0.4$ and 0.9 . The figure shows that regardless the value of η , when the TCC cavity is shorter than $L_C = 8\mu\text{m}$, both CNR and LF-RIN are comparable to those of the VCSEL without feedback; no noticeable excess noise is seen. In this case, the TCC VCSEL operates under stable CW operation for different values of coupling ratios. The same situation applies to the length range of $10\mu\text{m} < L_C < 13\mu\text{m}$. The shown enhanced values of LF-RIN and lowered values of CNR when $\eta = 0.4$ correspond to lengths resulting in regular and/or irregular oscillations.

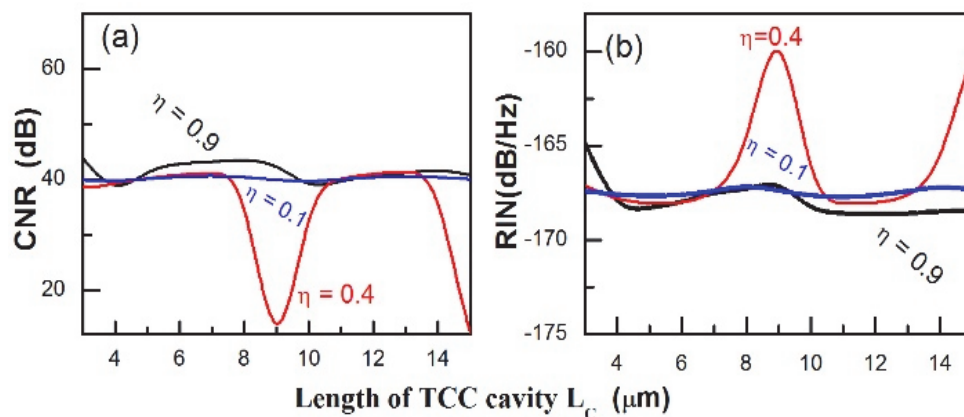


Fig. 8. (a) Variation of (a) CNR and (b) LF-RIN with the TCC length L_C .

3. CONCLUSIONS

We presented modeling and simulation of the dynamics and noise of VCSELs coupled to a transverse cavity, which is designed to operate at high speeds. The mechanism in which the TCC works to enhance the modulation bandwidth of the TCC VCSEL was modeled and explained. The modulation bandwidth can increase beyond 70 GHz when the length of the TCC is 3 μm and the coupling ratio is as large as 0.96. The noise performance of the TCC VCSEL is optimized when the VCSEL operates in CW, which is dominant when the length of the transverse cavity is lower than 8 μm and over the range of $10\mu\text{m} < L_C < 13\mu\text{m}$. When the TCC VCSEL emits regular and/or irregular oscillations RIN is enhanced and CNR is lowered.

REFERENCES

- [1] K. Iga, *Jpn. J. Appl. Phys.* **47**(1R), 1–10 (2008).
- [2] F. Koyama, *J. Lightw. Technol.* **24**(12), 4502–4513 (2006).
- [3] X. Zhao, D. Parekh, E. K. Lau, H.K. Sung, M. C. Wu, W. Hofmann, M. C. Amann, and C. J. Chang-Hasnain, *Opt. Exp.* **15**(22), 14810-14816 (2007).
- [4] S. H. Lee, D. Parekh, T. Shindo, W. Yang, P. Guo, D. Takahashi, N. Nishiyama, C. J. Chang-Hasnain, and S. Arai, *Opt. Exp.* **18**(16), 16370 (2010).
- [5] J. Harrison and A. Mooradian, *IEEE J. Quantum Electron.* **Vol. 25**, pp. 1152–1155, (1989).
- [6] J. M. Kahn, C. A. Burrus, and G. Raybon, *IEEE Photon. Technol. Lett.*, **Vol. 1**, pp. 159–161, (1989).
- [7] G. P. Agrawal and C. H. Henry, *IEEE J. Quantum Electron.*, **Vol. 24**, pp. 134–142, (1988).
- [8] G. Wenke, R. Gross, P. Meissner, and E. Patzak, *J. Light wave Technol.*, **Vol. 5**, pp. 608–615, (1987).

In Press, Accepted Manuscript – Note to users

- [9] H. Dalir and F. Koyama, *Appl. Phys. Lett.* **103(9)**, 091109 (2013).
- [10] H. Dalir and F. Koyamad, *IEICE Electron. Exp.* **8(13)**, 1075-1081(2011).
- [11] M. F. Ahmed, A. Bakry, R. Altuwirqi, M. S. Alghamdi, and F. Koyama, *Jpn. J. Appl. Phys.* **52(12)**, 124103(2013).
- [12] R. Lang and K. Kobayashi, *IEEE J. Quantum Electron.*, **Vol. QE-16**, pp. 347-355, (1980).
- [13] S. Abdulrhmann, M. Ahmed, T. Okamoto, W. Ishimori, M. Yamada, *IEEE. J. Quantum. Electron.* **Vol. 9**, PP. 1265–1274, (2003).
- [14] S. Abdulrhmann, M. Ahmed and M. Yamada, *SPIE*, vol. 4986, pp. 490-501, 2003.
- [15] J. Mork, Ph.D. Thesis., Technical University of Denmark, Denmark, (1988).
- [16] K. I. Kallimani and M. J. O. Mahony, *IEEE J. Quantum Electron.*, **Vol. 34**, pp. 1438-1446, (1998).
- [17] L. A. Coldren, S. W. Corzine, and M. L. Mashanovitch, **2nd ed.** New York, NY: Wiley, p. 260,(2012).
- [18] M. Ahmed, M. Yamada, and S. W. Z. Mahmoud, *Int. J. Numer. Model.*, **Vol. 20**, PP. 117-132, (2007).
- [19] M. Ahmed, N. Z. El-Sayed, and H. Ibrahim, *The European Physical Journal D*, **vol. 66**, no. 5, article 141,(2012).